A multiple comorbidities mouse lung infection model in *ApoE*-deficient mice

BENJAMIN BARTLETT[1,2], SILVIA LEE[1,3], HERBERT P. LUDEWICK[1,4], TECK SIEW[5,6], SHIPRA VERMA[5,7], GRANT WATERER[2,6], VICENTE F. CORRALES-MEDINA[8,9] and GIRISH DWIVEDI[1,2,10]

[1]Department of Advanced Clinical and Translational Cardiovascular Imaging, Harry Perkins Institute of Medical Research, Perth, Western Australia 6150; [2]School of Medicine, The University of Western Australia, Perth, Western Australia 6009; [3]Department of Microbiology, Pathwest Laboratory Medicine, Perth, Western Australia 6000; [4]Heart and Lung Research Institute, Harry Perkins Institute of Medical Research, Perth; [5]Department of Nuclear Medicine, Fiona Stanley Hospital, Perth, Western Australia 6150; [6]Royal Perth Hospital, Perth, Western Australia 6000; [7]Department of Geriatric Medicine, Fiona Stanley Hospital, Perth, Western Australia 6150, Australia; [8]Department of Medicine, University of Ottawa, Ottawa, ON K1N 6N5; [9]Clinical Epidemiology Program, The Ottawa Hospital Research Institute, Ottawa, ON K1H 8L6, Canada; [10]Department of Cardiology, Fiona Stanley Hospital, Perth, Western Australia 6150, Australia

Received August 4, 2022; Accepted December 9, 2022

DOI: 10.3892/br.2023.1603

Abstract. Acute pneumonia is characterised by a period of intense inflammation. Inflammation is now considered to be a key step in atherosclerosis progression. In addition, pre-existing atherosclerotic inflammation is considered to play a role in pneumonia progression and risk. In the present study, a multiple comorbidities murine model was used to study respiratory and systemic inflammation that results from pneumonia in the setting of atherosclerosis. Firstly, a minimal infectious dose of *Streptococcus pneumoniae* (TIGR4 strain) to produce clinical pneumonia with a low mortality rate (20%) was established. C57Bl/6 *ApoE*$^{-/-}$ mice were fed a high-fat diet prior to administering intranasally 10^5 colony forming units of TIGR4 or phosphate-buffered saline (PBS). At days 2, 7 and 28 post inoculation (PI), the lungs of mice were imaged by magnetic resonance imaging (MRI) and positron emission tomography (PET). Mice were euthanised and investigated for changes in lung morphology and changes in systemic inflammation using ELISA, Luminex assay and real-time PCR. TIGR4-inoculated mice presented with varying degrees of lung infiltrate, pleural effusion and consolidation on MRI at all time points up to 28 days PI. Moreover, PET scans identified significantly higher FDG uptake in the lungs of TIGR4-inoculated mice up to 28 days PI. The majority (90%) TIGR4-inoculated mice developed pneumococcal-specific IgG antibody response at 28 days PI. Consistent with these observations, TIGR4-inoculated mice displayed significantly increased inflammatory gene expression [interleukin (IL)-1β and IL-6] in the lungs and significantly increased levels of circulating inflammatory protein (CCL3) at 7 and 28 days PI respectively. The mouse model developed by the authors presents a discovery tool to understand the link between inflammation related to acute infection such as pneumonia and increased risk of cardiovascular disease observed in humans.

Correspondence to: Professor Girish Dwivedi, Department of Cardiology, Fiona Stanley Hospital, 11 Robin Warren Drive, Murdoch, Perth, Western Australia 6150, Australia
E-mail: girish.dwivedi@perkins.uwa.edu.au

Abbreviations: CAP, community acquired pneumonia; CCR, chemokine (C-C motif) receptor; CCL, chemokine (C-C motif) ligand; CFU, colony forming units; CVD, cardiovascular disease; ^{18}F-FDG, 2-deoxy-2-[fluorine-18]fluoro-D-glucose; H&E, hematoxylin and eosin; HFD, high fat diet; IFN, interferon; IL, interleukin; IP, intraperitoneal; IV, intravenous; MMP, matrix metalloproteinase; MRI, magnetic resonance imaging; PBS, phosphate-buffered saline; PCR, polymerase chain reaction; PET/CT, positron emission tomography/computed tomography; PI, post inoculation; RNA, ribonucleic acid; SUV, standardised uptake value; TNF, tumor necrosis factor

Key words: animal model, ApoE-deficient mice, atherosclerosis, cardiovascular disease, pneumonia

Introduction

Community-acquired pneumonia (CAP) is a common and potentially fatal infection of the lungs caused by bacteria or other pathogens (1). Accumulating studies demonstrate that patients who survive pneumonia have up to a 4-fold greater risk of cardiovascular disease (CVD) (i.e., myocardial infarction or stroke) in the first 30 days post infection; however, the risk of CVD complications can remain elevated ~2-fold for up to 10 years post-infection (2-5). While the mechanisms for the increased risk of CVD observed following CAP are unclear, it is also not known if pre-existing CVD (such as atherosclerosis) can modify the response of an individual to pneumonia infection. Studies indicate that dysregulated inflammatory activity related to CAP could be associated with the progression of

atherosclerosis and its CVD complications (2,6,7). Recent data suggest that pre-existing atherosclerotic inflammation can modulate pulmonary immunity or the immunopathogenesis of respiratory infections (8,9). Fang *et al* demonstrated that hypercholesterolemia induced by 12-16 weeks of a high fat diet (HFD) in wild-type C57BL/6J mice caused low grade pulmonary inflammation mediated by the activation of the toll-like receptor/nuclear factor kappa-light-chain-enhancer of activated B cells (TLR/NF-κB) pathways (8). Similarly, Ouyang *et al* showed that *ApoE*$^{-/-}$ mice on a HFD have increased pulmonary immune cell infiltration at 4 weeks, and increased lung cholesterol content and production of inflammatory mediators at 12 weeks (9). Compared to wild-type mice, the lungs of *ApoE*$^{-/-}$ mice infected with *Chlamydophilia pneumoniae (C. pneumoniae)* were revealed to have increased levels of interleukin (IL)-10, IL-6 and IL-4 and reduced cellular infiltration, whereas serum *C. pneumoniae*-specific IgG and IgM levels were increased (10).

The present study was conceived with the objective of investigating the longitudinal immune responses and changes in lung morphology that occur following induction of pneumonia with *Streptococcus pneumoniae* (*S. pneumoniae)* serotype 4 strain (TIGR4) in *ApoE*$^{-/-}$ mice and monitoring for up to 28 days post inoculation (PI). *S. pneumoniae* was selected because it is the most prominent cause of CAP in humans and is associated with significant morbidity and mortality worldwide (11). *ApoE*$^{-/-}$ mice were selected because this is an already well-established animal model of pre-clinical atherosclerosis in humans.

Material and methods

Animals. Two groups of *ApoE*$^{-/-}$ male mice aged 6-7 weeks were obtained from the Animal Resources Centre (West Australia, Australia) and maintained under pathogen-free conditions. A total of 75 male ApoE$^{-/-}$ mice, aged 6-7 weeks were obtained from the Animal Resources Centre (West Australia, Australia), housed in pairs and maintained under pathogen-free conditions. Mice were housed at 21˚C, 41% humidity and on a standard 12-h light/dark cycle. Animals were acclimated for 7 days with standard rodent chow before they were transitioned to a HFD containing 21% fat and 0.15% cholesterol (Fig. 1A and B) to accelerate development of atherosclerosis (Specialty Feeds). After 8 weeks of a HFD, atherosclerotic plaques were evident in the aortic arch of *ApoE*$^{-/-}$ mice (Fig. S1), as previously described (12). All animal experiments and procedures were approved by the local Ethics Committees of Harry Perkins Institute of Medical Research, Perth, Australia (approval no. AE114) and the University of Western Australia, Perth, Australia (approval no. F71731).

Bacterial culture. *S. pneumoniae* strain TIGR4 (gifted by Professor Gary Lee, University of Western Australia), was grown overnight on blood agar plates (with 5% sheep blood) or in brain heart infusion broth (both from Thermo Fisher Scientific, Inc.) at 37˚C in 5% CO_2 until OD_{600}=0.4. Aliquots of stock cultures in logarithmic growth were frozen in 10% glycerol (Sigma-Aldrich; Merck KGaA) and stored at -80˚C. Colony forming units (CFU) were determined by plating on blood agar plates and measuring the optical density. Bacteria were washed twice and diluted in phosphate-buffered saline (PBS; Thermo Fisher Scientific, Inc.) to obtain the appropriate concentrations for the mouse intranasal inoculation.

Intranasal inoculation. After 8 weeks of a HFD, mice were lightly anesthetized by inhalation with 3% isofluorane (Provet NZ Pty, Ltd.) and inoculated intranasally with 10^5 CFU of bacteria in a total volume of 40 μl. To determine the final dose, three factors were considered: i) The dose had to be sufficient to impose weight loss while allowing the mice the opportunity to recover from the infection; ii) the survival rate had to be >80%; and iii) pneumonia had to be detectable by magnetic resonance imaging (MRI) or positron emission tomography/computed tomography (PET/CT) imaging. The final dose was within the range of CFUs from similar mouse studies (10^4-10^6 CFU) (13-17), with comparable infection and survival rates and without antibiotic intervention. The dose was initially confirmed in two independent experiments of 10 mice to confirm the mortality rate and consistency in MRI imaging. Bacterial inoculation titres were confirmed by serial dilution and plating on blood agar plates. Control mice were challenged intranasally with 40 μl PBS. For the final experiment, a total of 75 mice were utilised: 55 mice were assigned for MRI imaging (Fig. 1A; TIGR4, n=30; PBS n=25) and the remaining 20 were assigned to PET imaging (Fig. 1B; TIGR4, n=11, PBS=9). Following inoculation, accommodations in temperature (heat pads) and supplementary fluids (hydration gel) were provided as necessary. The health of mice was monitored twice daily for the first 48 h PI and once daily thereafter up until a final time point of 28-days PI (total maximum experiment duration of 13 weeks). Health and disease severity were assessed via weight loss and scoring in any of the following areas: Respiration, body posture, eye condition, social interaction, and activity. Based on these criteria and a scoring system developed by the Animal Ethics Committee at Harry Perkins Institute of Medical Research, the mice were given a clinical score of healthy (0) to moribund (3). Any mice displaying a score above 3 were immediately humanely euthanized via cervical dislocation in accordance with our protocol. In total, 3 mice were euthanised due to severe *S. pneumoniae* TIGR4 infection and are further reported in the section *Intranasal inoculation and mice mortality*. Euthanasia was confirmed by loss of heartbeat and no response to foot pinch test.

Bacterial quantification in blood and lungs. Blood was collected from the tail vein, serially diluted in PBS and plated on blood agar plates. To determine bacterial burden in the lungs, supernatants of homogenised lungs were serially diluted in PBS and plated on blood agar plates. Plates were incubated for 18-24 h at 37˚C with 5% CO_2 and colonies were manually counted.

PET/CT imaging. Mice were fasted from food for 4-6 h (water available). The animals were warmed for 30 min (at approximately 30˚C) prior to administration of 2-deoxy-2-[fluorine-18] fluoro-D-glucose (18F-FDG). Anaesthesia with 3-5% isoflurane was administered until visible loss of consciousness and administration of ~20 MBq of 18F-FDG by either intravenous (IV) or intraperitoneal (IP) injection (volume <200 μl for IV

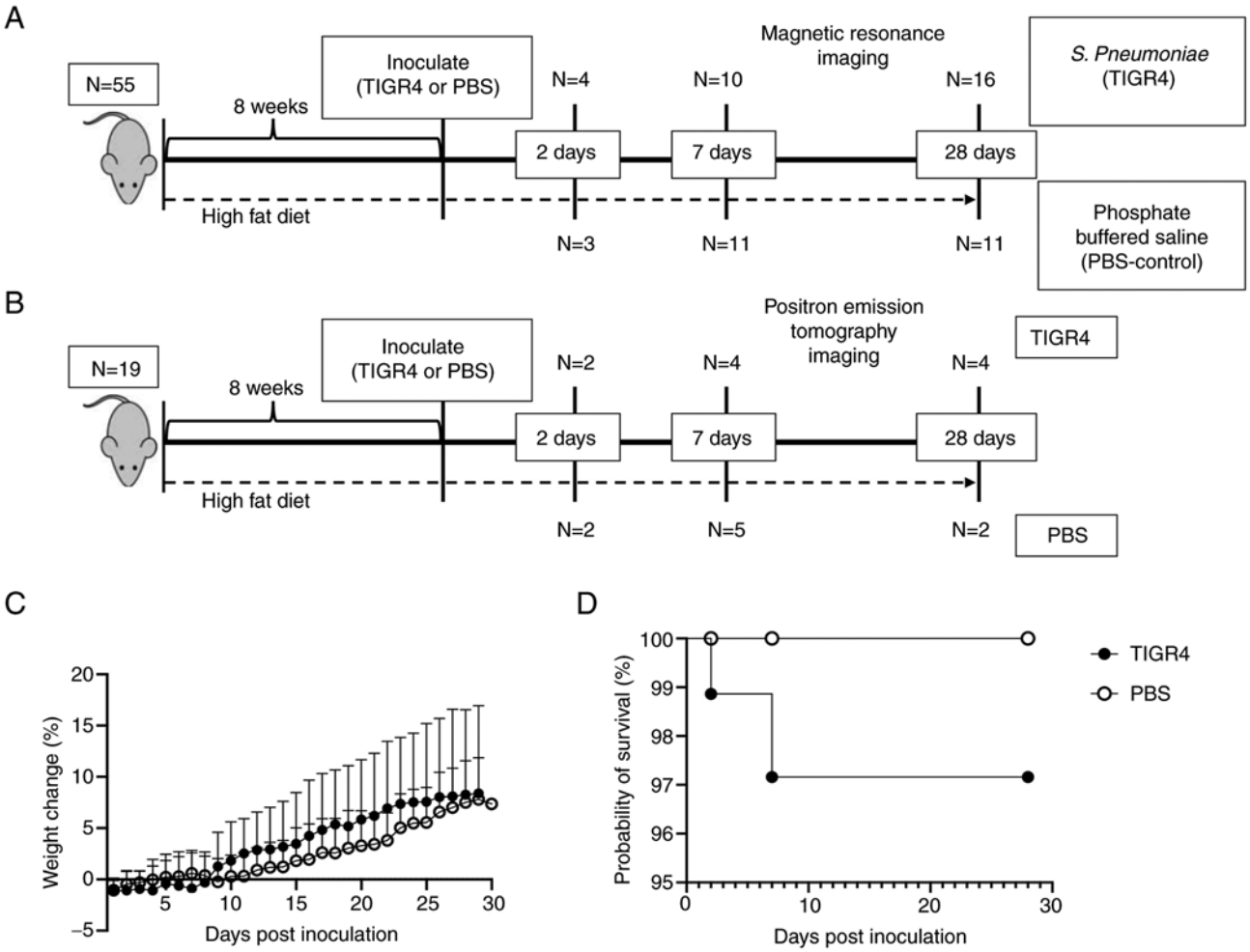

Figure 1. Body weight gain and survival rate. (A) Experimental flow chart. Mice underwent MRI at specific time points (2, 7 or 28 days PI). Blood was also collected before the switch to a HFD, 5 weeks into a HFD, pre-inoculation and at the study end-point (2, 7 or 28 days PI). (B) In parallel, a group of 19 mice were similarly treated but assigned for PET imaging. Due to the presence of radiotracer, only blood was collected prior to inoculation and imaging otherwise no tissues were harvested from these mice. (C) Weight loss of mice intranasally inoculated with 10^5 TIGR4 or PBS. (D) Survival curve of mice intranasally inoculated with TIGR4 or PBS. MRI, magnetic resonance imaging; PI, post inoculation; HFD, high fat diet; PET, positron emission tomography; PBS, phosphate-buffered saline.

injection). After completion of 1 h uptake, the mice were sacrificed via cervical dislocation, and PET/CT scan was completed using Bioscan BioPET/CT 105 camera (Bioscan, Inc.). Mice were sacrificed prior to imaging to reduce motion artifact from mouse orientation and movements and to overall improve image quality, and semi-quantitation. 18F-FDG-PET/CT scans were analysed by Syngio.via software (VB40; Siemens Healthineers).

MRI imaging. Upon reaching the assigned time point, mice were sequentially MRI imaged and euthanised. Mice were placed under anaesthesia with 3-5% isoflurane under warming conditions (~30˚C). Once the depth of anaesthesia was adequate, the mouse was moved to the imaging bed where the animal was imaged using the MR Solution MRI 3T scanner (MR Solutions). Based on the signal and image quality, a gadolinium-based contrast agent was administered to improve imaging quality if deemed required by the imaging technologist. Anaesthesia with isoflurane was maintained during the scan while respiration and vital signs were monitored remotely. InVivoScope software (Bioscan, Inc.) was used for image capture according to the Harry Perkins Cancer Imaging Facility licence.

Measurement of IgG levels by ELISA. *S. pneumoniae* TIGR4 was cultured in brain heart infusion broth, harvested at mid-log phase and washed twice with PBS. Nunc MaxiSorp 96 well plates (Thermo Fisher Scientific, Inc.) were coated overnight at 4˚C with 105 CFU per well of whole TIGR4 pneumococci in 100 μl of PBS. Plates were washed three times with 0.05% Tween/PBS and blocked for 1 h in blocking buffer (PBS with 5% skim milk) at room temperature. Serial 2-fold dilutions of serum in 2% skim milk/PBS were added to the well and incubated for 2 h at room temperature. After washing, pneumococcal-specific antibodies were detected by incubating with HRP-conjugated goat anti-mouse IgG Ab (cat. no. PA1-7259; Thermo Fisher Scientific, Inc.) diluted 1:10,000 in 2% skim milk/PBS for 1 h in the dark at room temperature. After washing five times with wash buffer, 3,3',5,5'-tetramethylbenzidine substrate (Sigma-Aldrich; Merck KGaA) was added and colour development was stopped after 15 min by the addition of H_2SO_4. Plates were read at 450 nm using an Omega plate

reader (BMG Labtech). The cut-off values were defined using average plus three standard deviations.

Histological analysis. Whole lungs were harvested and embedded in Tissue-Tek OCT (ProScitech) and immediately frozen to prevent tissue damage. Samples were stored at -80˚C. Subsequently, 10-μm sections were cut, air-dried and stained at room temperature unless otherwise described. Hematoxylin and eosin (H&E; cat. no. ab245880; Abcam) was completed as per the manufacturer's instructions. Briefly, sections were fixed in 100% MeOH for 3 min before staining with hematoxylin for 5 min, 2X ddH_2O wash, ~12 sec in bluing reagent, 2X ddH_2O wash, dipped in 100% EtOH, counterstained for 3 min in eosin and rinsed in 100% EtOH. Trichrome staining (cat. no. ab150686; Abcam) of the frozen sections was also performed according to the manufacturer's instructions with slight modification. The collagen stain, aniline blue, was replaced with 0.5% fast green in 70% EtOH (Sigma-Aldrich; Merck KGaA). This allowed for red, green and blue colour staining and subsequent colour deconvolution using ImageJ software (v1.53k; National Institutes of Health, Inc.) (18). Briefly, trichrome staining was completed following 3 min of MeOH fixing. First, the slides were incubated for 1 h in Bouin's fluid (included in trichrome staining kit, aforementioned) pre-heated to 54-64˚C, air cooled for 10 min, washed in ddH_2O until clear and incubated in Weigert's Iron Hematoxylin (included in H&E kit, aforementioned) for 5 min. Slides were rinsed in ddH_2O, stained with Biebrich Scarlet (included in trichrome staining kit, aforementioned) for 15 min, rinsed in ddH_2O, differentiated in phosphomolybdic acid for ~12 min, incubated in fast green for ~7 min, rinsed in ddH_2O and incubated in acetic acid for 3-5 min. H&E and trichrome-stained sections were mounted in aqueous mounting medium (Fronine Pty, Ltd.). Sections were imaged using a Nikon Eclipse TE2000-U microscope (Nikon Corporation).

Quantification of gene expression by reverse transcription-quantitative polymerase chain reaction (RT-qPCR). Ribonucleic acid (RNA) from lungs was extracted using TRIzol reagent (Thermo Fisher Scientific, Inc.) and reverse transcribed to complementary deoxyribonucleic acid (cDNA) using the Tetro cDNA Synthesis Kit (Meridian Bioscience) according to the manufacturer's recommendations. Messenger RNA (mRNA) levels of *GAPDH* (Mm99999915_g1), *HPRT* (Mm00446968_m1), *IL-6* (Mm00446190_m1), tumor necrosis factor-α (*TNFA*) (Mm00443258_m1), *IL-1β* (Mm00434228_m1), interferon-γ (*IFN-γ*) (Mm00801778_m1), *IL-10* (Mm00439614_m1), *IL-17A* (Mm00439618_m1), *IL-18* (Mm00434225_m1), NLR family pyrin domain containing 3 (*NLRP3*) (Mm00840904_m1), chemokine (C-C motif) ligand 2 (*CCL2*) (Mm00441242_m1), chemokine (C-C motif) receptor 2 (*CCR2*) (Mm00438270_01), SMAD family member 7 (*SMAD7*) (Mm00484742_m1), P2X purinoreceptor 7 (*P2X7*) (Mm00440582_m1) and tumor growth factor-β (*TGF-β*) (Mm01178820_m1) were determined by quantitative PCR using Taqman primers and probe and Taqman Gene Expression Master Mix (all from Applied Biosystems; Thermo Fisher Scientific, Inc.) on a Rotorgene 6000 (Qiagen, Inc.). Cycling conditions for TaqMan PCR were 2 min at 50˚C and 10 min at 95˚C followed by 45 cycles of 15 sec at 95˚C and 1 min at 60˚C. Samples were performed in triplicate. Data were analysed on the basis of the relative expression method with the formula relative expression $2^{-\Delta\Delta Cq}$, where the amount of the target gene was normalized first to the endogenous reference (HPRT and GAPDH) and then relative to a calibrator (control animal) (19).

Determination of the serum levels of soluble proteins by multiplex Luminex Assay. Blood was collected from the tail vein and centrifuged at 541 x g for 15 min at room temperature. Serum was collected and stored at -80˚C until use. Levels of the following soluble proteins: TNF-α, IFN-γ, IL-6, IL-1β, IL-5, IL-10, IL-17, CCL3, dickkopf (Dkk)-1 and matrix metalloproteinase (MMP)-12 were assayed using the multiplex Mouse Magnetic Luminex Assay (cat. no. LXSAMSM; R&D Systems, Inc.) according to the manufacturer's instructions. Quantification of proteins were determined using the Luminex 200™ System (Thermo Fisher Scientific Inc.) via xPONENT software 4.3 (Luminex, A DiaSorin Company). The levels of detection for each analyte are: CCL3, 0.45 pg/ml; Dkk-1, 31.8 pg/ml; IFN-γ, 1.85 pg/ml; IL-1β, 41.8 pg/ml; IL-5, 0.24 pg/ml; IL-6, 2.30 pg/ml; IL-10, 8.20 pg/ml; IL-17, 7.08 pg/ml; MMP-12, 0.42 pg/ml; and TNF-α, 1.47 pg/ml.

Statistical analysis. Data are expressed as the median (range). All statistical tests were performed with GraphPad Prism 7 (GraphPad Software, Inc.). The Kaplan-Meir method was used to compare survival rates. Mann-Whitney was used to compare two groups. Differences with P-values <0.05 were considered statistically significant.

Results

Intranasal inoculation and mice mortality. To investigate the impact of the selected inoculum of *S. pneumoniae* on the mortality of mice with atherosclerosis, *ApoE*$^{-/-}$ mice (n=74) were intranasally inoculated with either 10^5 CFU of *S. pneumoniae* (n=40) or PBS (control, n=34 after 8 weeks on a HFD (Fig. 1A and B). Most TIGR4-inoculated mice developed minor symptoms of infection including ruffled fur, reduced activity, enlarged nasal vestibule, arched backs and squinted eyes during the first 48-72 h PI. Despite a subtle change in weight loss (Fig. 1C), there was no significant evidence of higher mortality (Fig. 1D) in infected compared to uninfected *ApoE*$^{-/-}$ mice. A total of three mice succumbed to pneumococcal infection. The first mouse succumbed on day 2 PI and cultures of its blood and liver tissue yielded 8.0×10^5 CFU/ml and 5.3×10^5 CFU/ml of *S. pneumoniae*, respectively. The second succumbed on day 7 PI and while blood culture yielded no bacterial growth, cultures of lung and liver tissues yielded 3.7×10^5 CFU/ml and 3.3×10^5 CFU/ml of *S. pneumoniae*, respectively. The third mouse succumbed 2 days PI, yielding 4.3×10^5 CFU/ml growth in the lung and 3.7×10^5 CFU/ml growth in the liver. Macroscopic pathological features (e.g., hemorrhagic and mottling) of the lungs and spleen are shown in Fig. S1B and C. Bacterial growth and morphology are represented in Fig. S1D. These results confirmed that intranasal inoculation of 10^5 CFU bacteria produced mild mortality in *ApoE*$^{-/-}$ mice, with >95% survival.

Intranasal inoculation with S. pneumonia and bacterial burden in tissues and blood. Blood and lung tissues were collected at 2, 7 and 28 days PI. No bacteria were recovered from the lungs and there was no evidence of bacteraemia in infected *ApoE*$^{-/-}$ mice that survived until the endpoints of the study. This observation is in line with previous research of low dose pneumonia in C57Bl/6 mice. Sender *et al* recovered only 2% of bacteria via bronchoalveolar lavage 6 h post-intratracheal injection of 10^5 TIGR4 bacteria in C57Bl/6 mice (20).

Ongoing inflammation on FDG PET/CT imaging. Evaluation of mouse lung PET/CT scans was performed by a level 3 trained nuclear medicine specialist (SV), who was blinded to the study groups and designations. Representative PET/CT scans are presented in Fig. 2. In line with previous PET imaging in patients with pneumonia (21), of the 20 mice assigned to PET imaging, all 11 mice that received an intranasal dose of TIGR4 bacteria presented with increased FDG uptake [standardised uptake value (SUV)] in the lungs compared to PBS-inoculated mice (n=8) at 7 days PI (Fig. 3A and B). Of note, at 7-days PI there was a significant increase (P=0.0159 at 7 days) in both the average and maximum lung SUVs in TIGR4-inoculated mice compared to PBS. In addition, one PBS mouse was excluded from the study due to the presence of a genetic heart defect.

Intranasal inoculation of S. pneumoniae and lung changes on MRI. Evaluation of mouse lungs was performed by a level 3 trained radiologist (TS), who was blinded to the study groups and designations. The two mice that succumbed to the TIGR4 infection were not imaged. Of the four TIGR4-inoculated mice that underwent MRI at 2 days PI, three presented radiological findings consistent with lung infection including pleural effusion, consolidation, and various degrees of lung infiltration. In total, 4/8 (50%) TIGR4-inoculated mice scanned at 7 days PI, and 6/15 (40%) TIGR4-inoculated mice scanned at 28 days PI presented with the characteristics described above. None of the PBS-inoculated mice presented with any lung radiological abnormalities that would suggest a respiratory infection. Hence, across all time points, 13 of the 27 mice inoculated with *S. pneumoniae* presented with radiological findings suggestive of pulmonary infection (Fig. 4). The weight the mice that were positive for lung infection were compared to the weights of the remaining TIGR4 mice (Fig. S2K).

Pneumococcal-specific IgG antibody responses. At 2 days PI, one TIGR4-inoculated mouse produced a low level of pneumococcal-specific IgG antibody (Fig. 5A). No antibody responses were recorded in TIGR4-inoculated mice at 7 days PI (Fig. 5B). By contrast, 15/17 (88%) TIGR4-inoculated mice developed an antibody response (Fig. 5C; P<0.0001) at 28 days PI. Pneumococcal-specific IgG antibodies were not detected in any of the PBS-inoculated animals. These results are consistent with IgG antibody kinetics to *S. pneumonia* infection (22) and demonstrated that the inoculating dose selected for this study was sufficient to elicit antigen-specific antibody responses.

Lung pathology. H&E staining revealed lung remodelling consistent with previous studies in *ApoE*$^{-/-}$ mice (23,24), however this appeared exacerbated in TIGR4-inoculated mice. Progressively, alveolar space and nuclei density increased 2-, 7- and 28-days PI, with the greatest difference observed at 28 days PI (Fig. 6A). Compared to PBS-inoculated animals, TIGR4-inoculated mice demonstrated increased alveolar septal thickness, suggestive of increased immune cell infiltration. Despite increased lung density and infiltration, there was no significant difference in collagen presence detected in the lungs of TIGR4- and PBS-inoculated mice (Fig. 6B).

Increased IL-1β and IL-6 gene expression in the lungs of ApoE$^{-/-}$ *mice infected with S. pneumoniae*. *IL-1β* gene expression was significantly increased in the lungs of TIGR4-inoculated mice compared to control mice at 7 days PI (P=0.002; Fig. 7A). *IL-6* gene expression was also significantly higher in TIGR4-inoculated mice at 28 days PI (P=0.01; Fig. 7B). There was also a trend for elevated *IL-1β* (P=0.09) and *TNF-α* (P=0.11) gene expression in TIGR4-inoculated mice at 28 days PI (Fig. 7A and D). By contrast, a trend towards decreased *IFN-γ* gene expression (P=0.09) was evident in TIGR4-inoculated mice at 7 days (Fig. 7E). There was no difference in *TGF-β* gene expression in lung tissues between TIGR4- and PBS-inoculated mice at any of the time points (Fig. 7C), confirming the immunohistochemistry collagen results. Gene expression for *CCR2, CCL2, IL-10, IL-17, IL-18, NLRP3, P2X7* and *SMAD7* were similar in TIGR4- and PBS-inoculated mice (Fig. S3). Mice positive for respiratory infection confirmed by MRI were compared to the remaining TIGR4 mice, and exhibited an increasing trend for *IL-6, TNF-α, IL-1, NLRP3* and *CCL2* at 7 days before decreasing at 28 days PI (Fig. S2). The results indicated residual local inflammatory dysregulation in mice inoculated with *S. pneumoniae* despite no bacterial burden in the lungs.

Increased circulating levels of IL-6 and CCL3 in ApoE$^{-/-}$ *mice infected with S. pneumoniae*. There were no significant differences observed in the serum levels for any of the soluble proteins at 2 days PI between TIGR4- and PBS-inoculated mice. At 7 days PI, levels of IL-6 were significantly higher in TIGR4-inoculated mice compared to mice inoculated with PBS (Fig. 8E; P=0.0165). At 28 days PI, CCL3 levels were significantly higher in TIGR4-inoculated mice compared to mice inoculated with PBS (Fig. 8B; P=0.007). No differences were observed for levels of Dkk-1 and MMP-12 between TIGR4- and PBS-inoculated mice at 7- and 28-days PI (Fig. 8A and H). In most samples, IL-5, IL-1β, IL-10 and IL-17 were below the levels of detection (Fig. 8C, D, F and G), whereas TNF-α and IFN-γ were undetectable for all the mice (data not shown). The results indicated ongoing heightened systemic inflammatory activity in mice inoculated with *S. pneumoniae* despite clearance of bacterial infection.

Discussion

To the best of our knowledge, this is the first study to establish a longitudinal model of *S. pneumoniae* infection without antibiotic rescue to explore the pulmonary and systemic pathology in *ApoE*$^{-/-}$ mice beyond the acute phase of the infection and well into the clinical recovery of surviving animals.

It has been proposed that the introduction of a respiratory infection leads to a mounting synergistic inflammatory

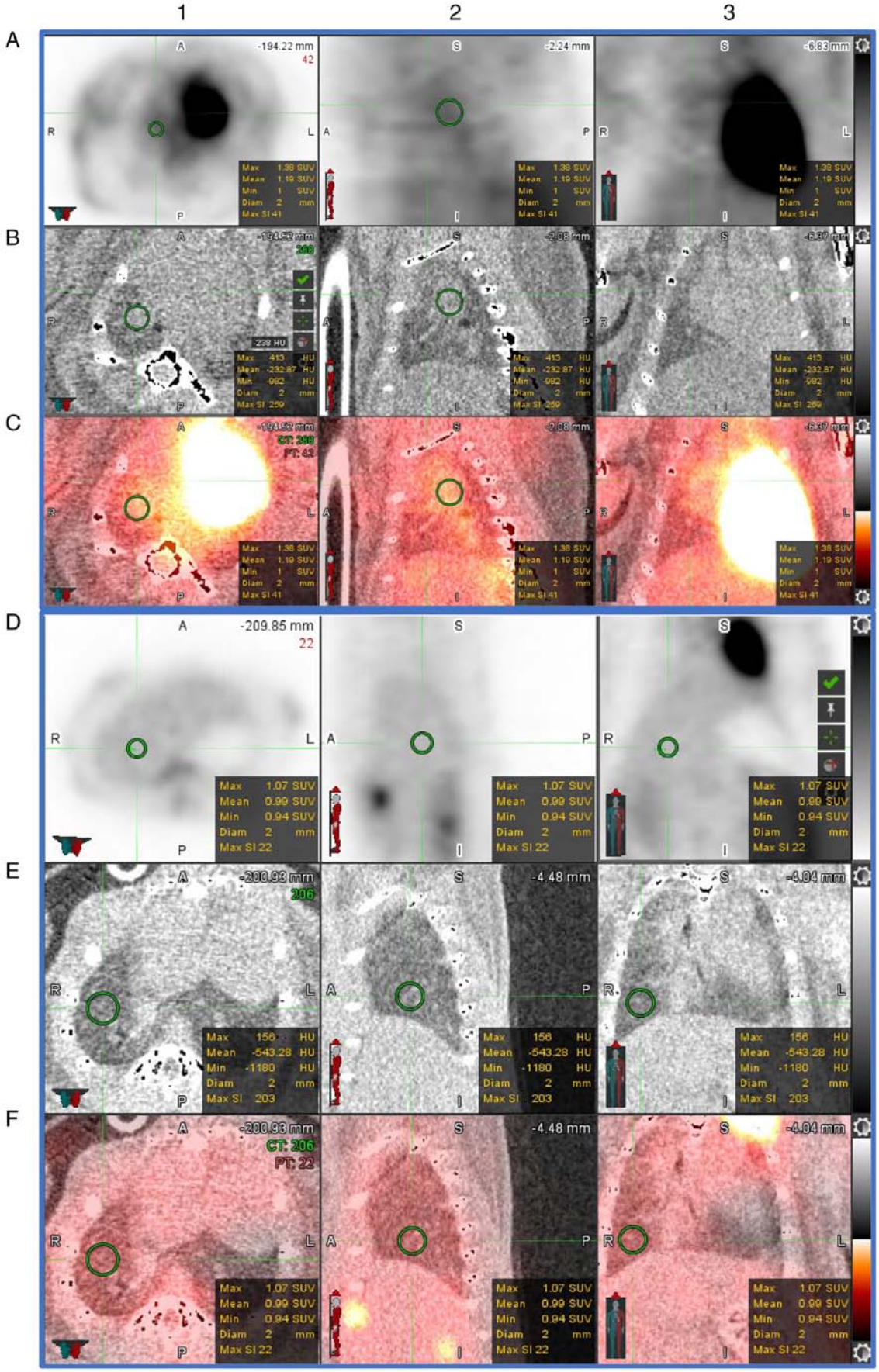

Figure 2. FDG-PET images from TIGR4 *Streptococcus*-infected mice. (A-C) Representative images from a TIGR4-infected mouse at 28 days PI. (D-F) Representative images from a PBS-inoculated mouse at 28 days PI. Rows A and D are PET scan, B and E are CT for localisation, and C and F are fused PET and CT scans. Regions of interest in row C demonstrated increased FDG uptake in TIGR4-inoculated mice compared to PBS inoculated mice (row F). PET, positron emission tomography; PI, post inoculation; PBS, phosphate-buffered saline; PET, positron emission tomography; CT, computed tomography; FDG, fluorodeoxyglucose.

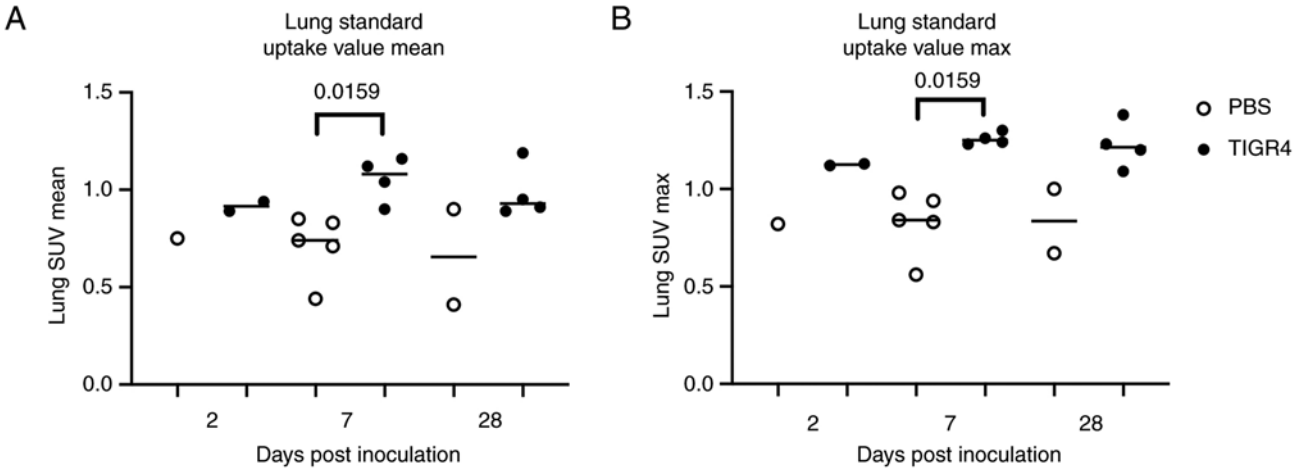

Figure 3. Average and maximum lung standardised uptake values on PET imaging. Across all time points there was increased fluorodeoxyglucose uptake in the lung of TIGR4-inoculated mice compared to PBS-inoculated mice. (A and B) At 7-days post inoculation there was a significant increase (P=0.0159) in TIGR4-inoculated mice compared to PBS in both the average and maximum lung standardised uptake values. PET, positron emission tomography; PBS, phosphate-buffered saline; SUV, standardised uptake values.

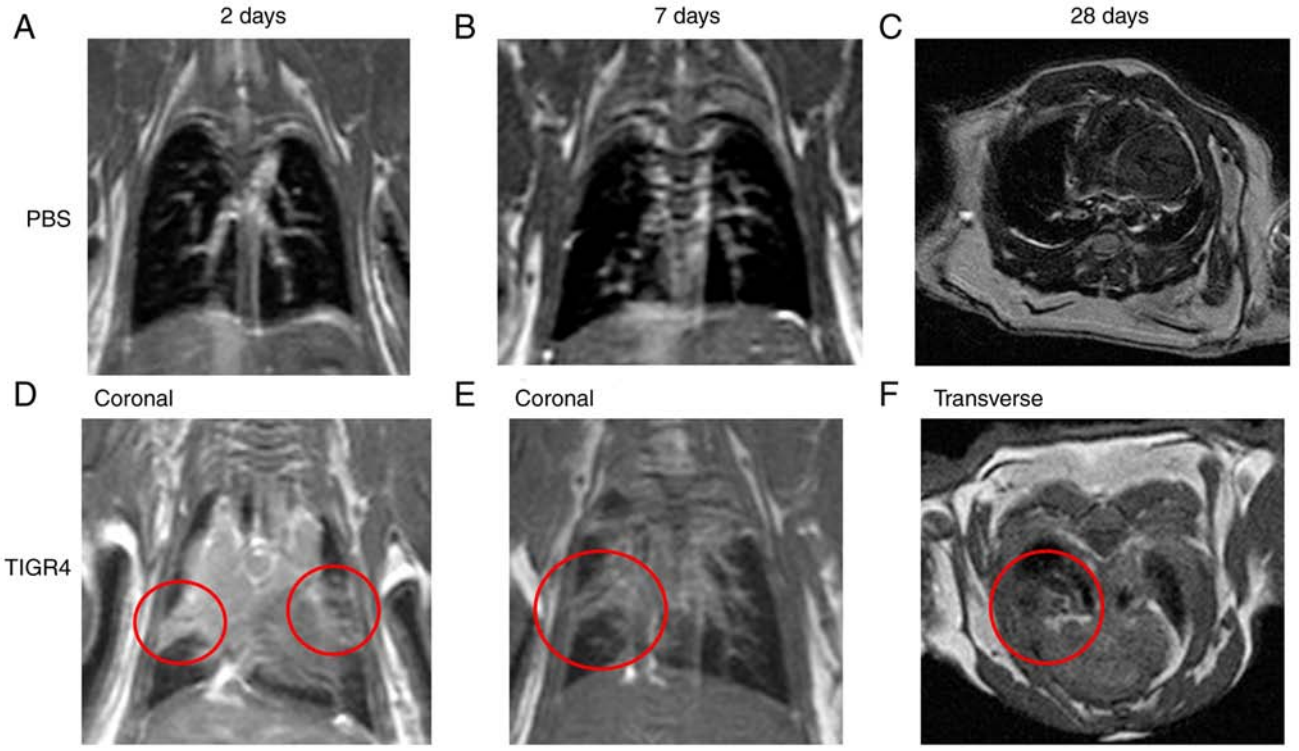

Figure 4. MRI of the lungs. (A and D) Representative images of mouse lungs from a PBS- and TIGR4-inoculated mouse at 2 days PI. ROI in D, demonstrates left and right lung consolidation with infiltration in the TIGR4-inoculated mouse. (B and C) Representative images of lungs from a PBS- and TIGR4-inoculated mouse at 7 days PI. ROI highlighted in (E) displays infiltrate in the right middle lobe. (C and F) Representative images of lungs from a PBS- and TIGR4-inoculated mouse at 28 days PI. ROI in F, demonstrates pleural effusion in the right lung. All scans shown are T1 weighted images. MRI, magnetic resonance imaging; PBS, phosphate-buffered saline; PI, post inoculation; ROI, region of interest.

response that could lead to adverse cardiovascular events. In CAP, exposure of alveolar epithelial cells and resident macrophages to *S. pneumoniae* stimulates the production of inflammatory cytokines such as IL-1β, IL-6 and TNF-α , as well as chemokines (25-28). The duration and magnitude of the inflammatory response have been linked to disease severity and clinical outcome. In a longitudinal study of 247 hospitalised patients with CAP, cytokine and chemokine levels were highest at hospital admission and while most decreased at 6-week follow-up, some markers remained elevated (29), suggesting ongoing residual inflammation. This was confirmed in a recent study of 22 CAP survivors, with 68% of subjects displaying increased ^{18}FDG uptake in the lungs, 30 to 45 days after their hospital discharge (21).

In agreement with these observations, TIGR4-inoculated mice displayed delayed elevated inflammatory response in the

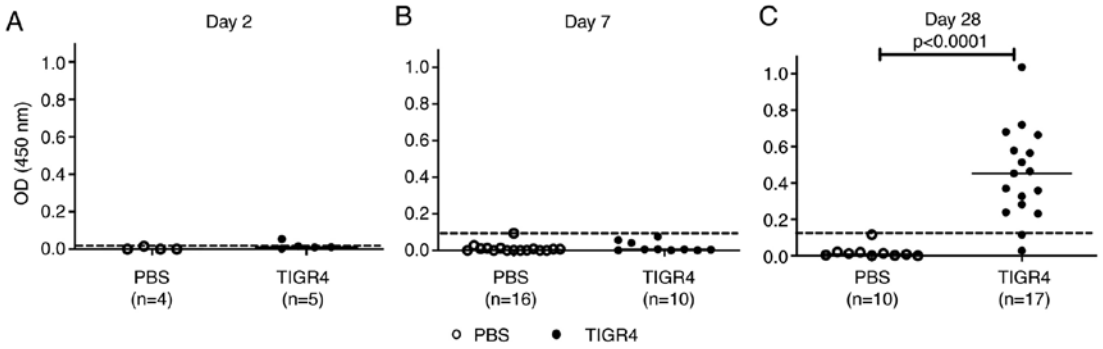

Figure 5. *S. pneumoniae*-specific serum antibody levels. Blood was collected from phosphate-buffered saline (control) or TIGR4-inoculated mice at specific PI time points: (A) 2 days PI, (B) 7 days PI and (C) 28 days PI. Dotted horizontal line represents average + 3x standard deviation. Solid horizontal line represents the median. PI, post inoculation; PBS, phosphate-buffered saline; OD, optical density.

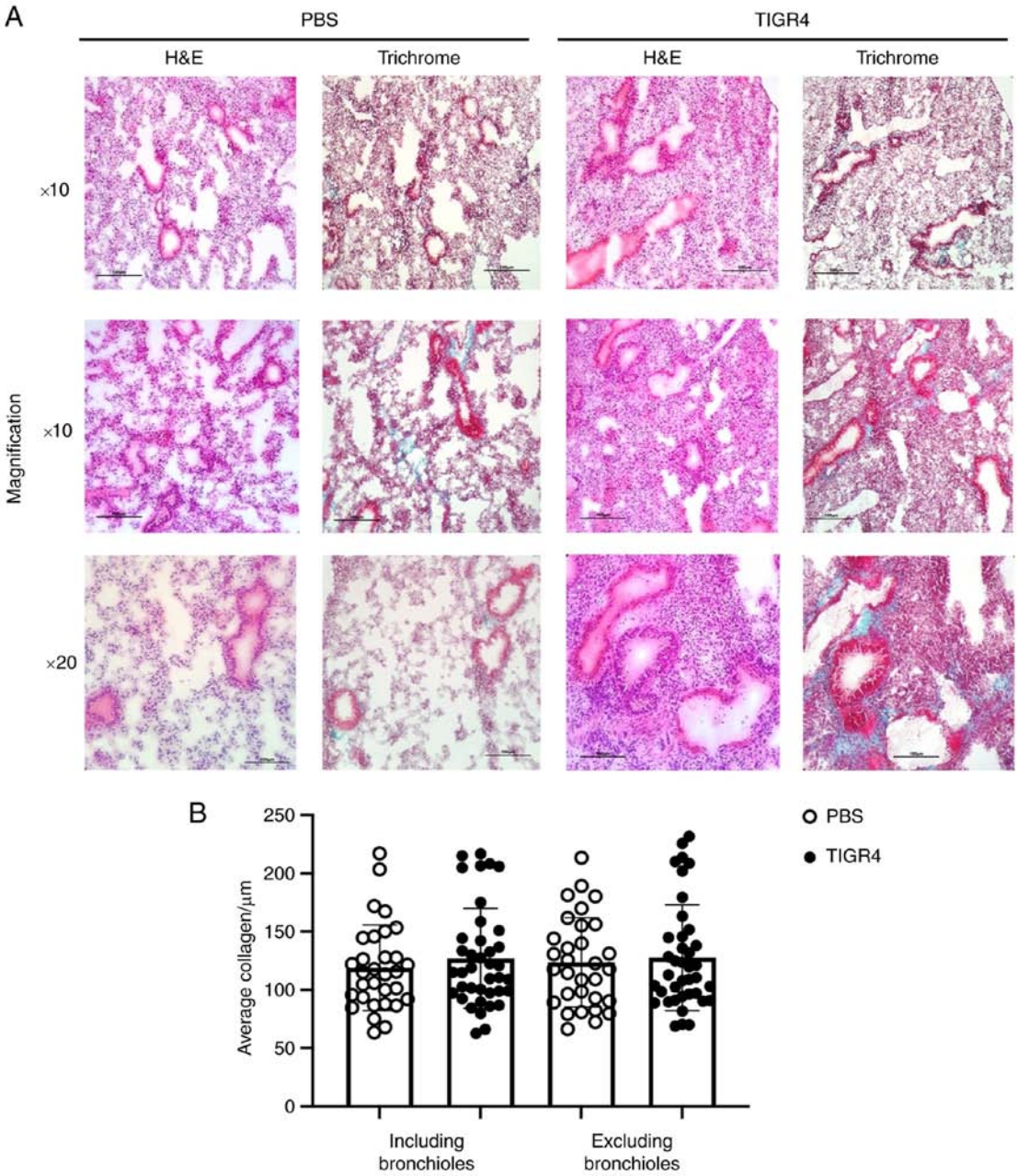

Figure 6. Representative images of lung remodelling in TIGR4- and PBS-inoculated mice at 28 days post inoculation. (A) Tissue sections were stained with hematoxylin and eosin or Trichrome. Rows 1 and 2 captured at a magnification of x10, and row 3 captured at a magnification of x20. All magnification bars represent 100 μm. (B) Average lung collagen content per μm in TIGR4- and PBS-inoculated mice including and excluding bronchioles. PBS, phosphate-buffered saline; H&E, hematoxylin and eosin.

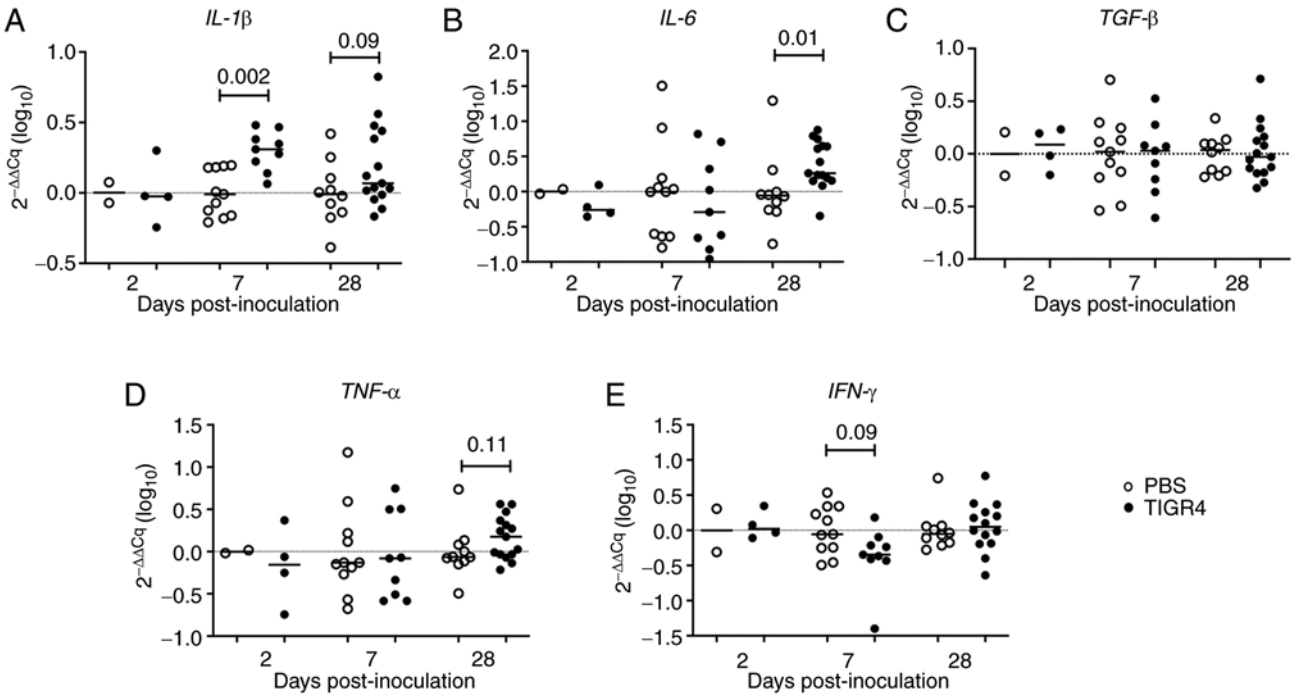

Figure 7. Gene expression of inflammatory mediators in the lungs. Phosphate-buffered saline control or TIGR4-inoculated mice were sacrificed at specific time points and RNA was extracted from lung tissues. mRNA expression levels of (A) *IL-1β*, (B) *IL-6*, (C) *TGF-β*, (D) *TNF-α*, and (E) *IFN-γ* were quantified by real-time polymerised chain recation PCR and normalised against two housekeeping genes (GAPDH and HPRT). The solid horizontal line represents the median and the dotted line represents no change in gene expression. RNA, ribonucleic acid; PBS, phosphate-buffered saline; *IL-1β*, interleukin-1β; *IL-6*, interleukin-6; *TGF-β*, tumor growth factor-β; *TNF-α*, tumor necrosis factor; *IFN-γ*, interferon-γ.

lungs (e.g., IL-6 at 28 days PI) and systemically (e.g., CCL3 at 28 days PI). Interestingly, systemic levels of IL-6 peaked at 7 days PI. IL-6 plays an important role in linking innate to an acquired immune response by promoting differentiation of naïve $CD4^+$ T cells (30). IL-6 can serve as an activator for other pro-inflammatory cytokines including IL-1 and TNF-α (31).

In response to an infection, IL-6 stimulates a range of signalling pathways including NF-κB, enhancing the transcription of the mRNA of inflammatory cytokines including IL-6, TNF-α, and IL-1β. TNF-α and IL-1β in turn also activate transcription factors to produce more IL-6 (32).

A study published by Bacci *et al* correlated increased IL-6 and TNF-α with worse outcomes in patients with pneumonia (31). While TNF-α and IL-6 gene expression in the lungs of TIGR4-inoculated mice at 28 days was not statistically significant, results do appear to show an upward trend. This could be attributed to the low TIGR4 dose, delivery and/or efficacy of the immune system response. Regardless, patients discharged with pneumonia leave hospital with ongoing subclinical inflammation (33), and in an $ApoE^{-/-}$ model of bacterial tuberculosis (34), there is a delayed adaptive immune response. Therefore, it is possible in the present study that not enough time PI had lapsed and a later time point may be worth investigating to elucidate long-term pneumonia-mediated inflammatory changes.

Neutrophils play a key role in response to controlling a pneumococcal pneumonia infection (35). CCL3 acts as a chemotactic factor for different leukocyte subsets and has also been shown to increase during development of atherosclerotic lesions (36,37). It has been shown that during acute inflammation triggered by lipopolysaccharide stimulation, CCL3 induces chemotaxis for neutrophils to atherosclerotic lesions (37). The data in the present study revealed the induction of CCL3 in response to an acute infection that may support atherosclerosis disease progression (Fig. 8B). Altogether there is great overlap in immune response to atherosclerosis and pneumonia, sharing a lot of the same immune pathways that could be pathologically relevant for atherosclerotic progression.

Previously associated with lung fibrosis, epithelial cell proliferation, acute lung inflammation, increased atherosclerotic apoptosis and enlarged and destabilized plaques, Dkk-1 has been identified in both a respiratory infection and atherosclerosis setting (38,39,40). Due to the majority of Dkk-1 being platelet-produced and its involvement in atherosclerosis, it has been recently suggested as an independent risk factor for major adverse cardiovascular events (40). A progressively increasing median of Dkk-1 was measured in TIGR4-inoculated mice compared to PBS (Fig. 8A).

In terms of lung fibrosis, a HFD and deletion of the *ApoE* gene can induce morphological changes to the lungs including lipidosis, increased pulmonary inflammation and an increase in alveolar septal thickness (9,24,41). These are consistent with findings in this model, with altered lung morphology in PBS-inoculated mice in response to hypercholesterolemia, and TIGR4-inoculated mice presenting with more severe remodelling as a result of inflammatory infiltrate caused by TIGR4 inoculation. The lungs of TIGR4-inoculated mice exhibited increased nuclei and inflammatory gene expression indicating an elevated sublethal amount of inflammation. While no difference in systemic Dkk-1 or lung collagen was detected, it could be argued that *S. pneumoniae* affects specific collagen groups and overall staining of the classical fibrillar and

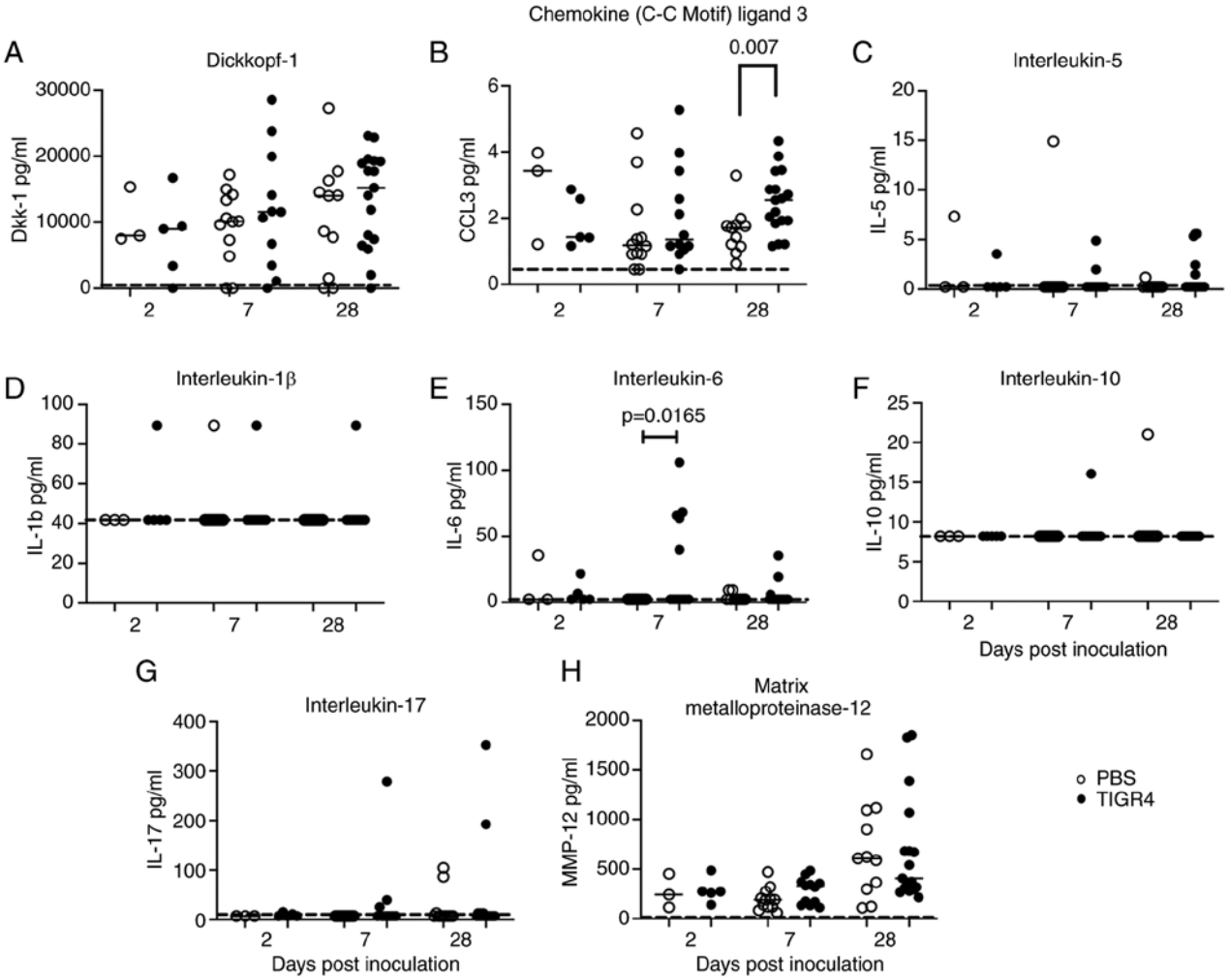

Figure 8. Circulating levels of soluble proteins. Blood was collected from phosphate-buffered saline (control) or TIGR4-inoculated mice at specific time points. Levels of circulating (A) dickkopf-1, (B) chemokine (C-C motif) ligand 3 (also known as macrophage inflammatory protein 1-α, (C) interleukin-5, (D) interleukin-1β, (E) interleukin-6, (F) interleukin-10, (G) interleukin-17, and (H) matrix metalloproteinase-12 were assessed. Horizontal line represents the median. Dotted line represents minimum level of detection of the Luminex assay. N values: 2 days post inoculation: Inf=5 and Control=3; 7 days post inoculation: Inf=12 and Control=12; 28 days post inoculation: Inf=17 and Control=11. PBS, phosphate-buffered saline.

network-forming collagen may not be entirely representative of the disease state. Moreover, the novel Dkk-1 biomarker requires further investigation to validate its clinical relevance in pneumonia and role in prediction of adverse events.

To date, few alternative multiple comorbidities animal models of acute pneumonia infection and atherosclerosis have been described (13,17,42-45), and a model of unstable plaque (46). In contrast to the model in the present study, these other models utilise surgical intervention (46), viral pathogens (e.g., influenza virus) (43), alternative routes of infection (e.g., intraperitoneal) that are more relevant to sepsis than pneumonia (44), intervene with antibiotics to improve mortality (13,17), or do not describe the lung pathology associated with the infectious challenge (13,17). The model of the present study utilises a low infectious dose to establish infection with *S. pneumoniae*, the most important bacterial cause of pneumonia in humans (25,47,48), via intranasal inoculation; hence, being representative of the pneumococcal infection that is acquired via the respiratory route in humans. Additionally, the respiratory infection was characterised via MRI and PET imaging modalities. The method used in the present study produces a model with a range of pathology that includes no detectable illness, subclinical disease, clinical infection, and infection-induced death thus resembling the full scope of pathology produced by exposure to respiratory pathogens in humans. Finally, by foregoing antibiotics, no putative additional confounder was introduced from such bioactive compounds (for example, some antibiotics such as macrolides, tetracyclines and fluoroquinolones can exert important anti-inflammatory activity) (49-51).

There are some limitations associated with the present study. Firstly, the cellular immune responses in the lungs that may have shed light on the lack of bacterial recovery from the lung, were not investigated. As a low dose of TIGR4 bacteria was administered to achieve low mortality in the animal model, it is likely that the bacteria were cleared quickly by the immune system precluding us from bacterial recovery from lungs. Indeed, the pre-existing inflammatory response activated by atherosclerosis may have helped to clear the low intranasal dose of *S. pneumoniae* TIGR4. The significant increase in pneumococcal-specific antibody response observed at 28 days PI is in agreement with the strong systemic CCL3

response indicative of exposure to *S. pneumoniae* supporting this hypothesis, however this will require further investigation with wild-type mice used as a control. The absence of the use of wild-type mice as a control is a limitation of the present study and should be addressed in future investigations.

Overall, the TIGR4 strain, used in studies by the authors, is an invasive strain that has been shown to cause pneumonia and lethal systemic disease following intranasal challenge (13-15,17,52). The utility of MRI and PET imaging modalities to diagnose respiratory infection, while somewhat limited with resolution in murine studies, are sufficient and valuable in supporting the diagnosis and investigation of respiratory and vascular disease (53).

In summary, the *ApoE*$^{-/-}$ mouse model of the present study utilising an intranasal inoculation of *S. pneumoniae* offers a representation of pneumonia infection in humans with subclinical atherosclerotic disease. The model is relevant to the study of pneumonia infections and characterisation of lung and systemic changes that occur following an episode of pneumonia in the context pre-existing atherosclerosis. This multiple comorbidity murine model will be useful in assessing cardiovascular risk following exposure to *S. pneumoniae*-caused pneumonia (12).

Acknowledgements

The authors gratefully acknowledge Mr Lincoln Codd (Charles Gairdner Hospital, Perth, Australia), Mr Brenton O'Mara (Charles Gairdner Hospital), Ms Kirsty Richardson (Harry Perkins Institute of Medical Research, Perth, Australia), Dr Liesl Celliers (Harry Perkins Institute of Medical Research), Dr Penny Maton (University of Western Australia, Perth, Australia) and Professor Roslyn J. Francis (University of Western Australia) for technical assistance. The authors acknowledge the facilities, and the scientific and technical assistance of Microscopy Australia at the Centre for Microscopy, Characterisation and Analysis, The Cancer Imaging Facility at Harry Perkins Institute of Medical Research, The University of Western Australia, a facility funded by the University, State and Commonwealth Governments.

Funding

The present study was funded by the Harry Perkins Institute of Medical Research. BB received funding from the Australia-India Strategic Research Fund (AISRF; grant no. AIRXIIICO000068) held by GD.

Availability of data and materials

The datasets used and/or analysed during the current study are available from the corresponding author on reasonable request.

Authors' contributions

The study was initially conceived by GW, VCM and GD. The study was developed from a combined effort of BB, SL, HPL, GW, VCM and GD. All animal work and subsequent experiments were completed by BB, SL and HPL. MRI and FDG-PET imaging analysis was completed by TS, SV, GW, VCM and GD. Manuscript preparation was performed by BB. Revisions and assessment for intellectual content was completed by SL, HPL, TS, SV, GW, VCM and GD. SL, HPL, TS and SV confirm the authenticity of all the raw data. All authors read and approved the final manuscript and agree to be accountable for all aspects of the research in ensuring that the accuracy or integrity of any part of the work are appropriately investigated and resolved.

Ethics approval and consent to participate

All animal procedures were carried out in accordance with the Western Australian Animal Welfare Act, National Institute of Health guidelines and ARRIVE guidelines. The present study and its procedures were approved by the Animal Ethics Committee of the Harry Perkins Institute for Medical Research, Perth, Australia (approval no. AE114) and the University of Western Australia, Perth, Australia (approval no. F71731). All handling, procedure and assistance techniques training was provided by the Bioresources team at the Harry Perkins Institute for Medical Research centre.

Patient consent for publication

Not applicable.

Competing interests

GD is Wesfarmers Chair in Cardiology at the University of Western Australia with an Adjunct Professor appointment at UOHI. GD reports 3 paid lectures from AstraZeneca, Pfizer, and Amgen not related to the topic in the manuscript. GD provides consultancy services and also has an equity interest Artrya Pty Ltd. The other authors (BB, SL, HPL, TS, SV, VFCM and GW) have nothing to disclose and declare that they have no competing interests.

References

1. Asthma, chronic obstructive pulmonary disease and other respiratory diseases in Australia, Summary. *Australian Institute of Health and Welfare* https://www.aihw.gov.au/reports/chronic-respiratory-conditions/asthma-chronic-obstructive-pulmonary-disease-and/summary.
2. Corrales-Medina VF, Alvarez KN, Weissfeld LA, Angus DC, Chirinos JA, Chang CCH, Newman A, Loehr L, Folsom AR, Elkind MS, *et al*: Association between hospitalization for pneumonia and subsequent risk of cardiovascular disease. JAMA 313: 264-274, 2015.
3. Corrales-Medina VF, Taljaard M, Yende S, Kronmal R, Dwivedi G, Newman AB, Elkind MSV, Lyles MF and Chirinos JA: Intermediate and long-term risk of new-onset heart failure after hospitalization for pneumonia in elderly adults. Am Heart J 170: 306-312, 2015.
4. Corrales-Medina VF, Taljaard M, Fine MJ, Dwivedi G, Perry JJ, Musher DM and Chirinos JA: Risk stratification for cardiac complications in patients hospitalized for community-acquired pneumonia. Mayo Clinic Proc 89: 60-68, 2014.
5. Corrales-Medina VF, Musher DM, Shachkina S and Chirinos JA: Acute pneumonia and the cardiovascular system. Lancet 381: 496-505, 2013.
6. Corrales-Medina VF, Musher DM, Wells GA, Chirinos JA, Chen L and Fine MJ: Cardiac complications in patients with community-acquired pneumonia clinical perspective: Incidence, timing, risk factors, and association with short-term mortality. Circulation 125: 773-781, 2012.

7. Bartlett B, Ludewick HP, Lee S and Dwivedi G: Cardiovascular complications following pneumonia: Focus on pneumococcus and heart failure. Curr Opin Cardiol 34: 233-239, 2019.
8. Fang Y, Wang S, Zhu T, Zhang Y and Lian X: Atherogenic high cholesterol/high fat diet induces TLRs-associated pulmonary inflammation in C57BL/6J mice. Inflamm Res 66: 39-47, 2017.
9. Ouyang Q, Huang Z, Lin H, Ni J, Lu H, Chen X, Wang Z and Lin L: Apolipoprotein E deficiency and high-fat diet cooperate to trigger lipidosis and inflammation in the lung via the toll-like receptor 4 pathway. Mol Med Rep 12: 2589-2597, 2015.
10. Nazzal D, Therville N, Yacoub-Youssef H, Garcia V, Thomsen M, Levade T, Segui B and Benoist H: Apolipoprotein E-deficient mice develop an anti-chlamydophila pneumoniae T helper 2 response and resist vascular infection. J Infect Dis 202: 782-790, 2010.
11. Ramos-Sevillano E, Ercoli G and Brown JS: Mechanisms of naturally acquired immunity to streptococcus pneumoniae. Front Immunol 10: 358, 2019.
12. Bartlett B, Ludewick HP, Verma S, Corrales-Medina VF, Waterer G, Lee S and Dwivedi G: Cardiovascular changes after pneumonia in a dual disease mouse model. Sci Rep 12: 11124, 2022.
13. Bazaz R, Francis S and Dockrell D: 215 increased atherosclerotic plaque macrophage content following streptococcus pneumoniae pneumonia. Heart 101: A117-A118, 2015.
14. Ghanem ENB, Maung NHT, Siwapornchai N, Goodwin AE, Clark S, Muñoz-Elías EJ, Camilli A, Gerstein RM and Leong JM: Nasopharyngeal exposure to streptococcus pneumoniae induces extended age-dependent protection against pulmonary infection mediated by antibodies and CD138+ cells. J Immunol 200: 3739-3751, 2018.
15. Ritchie ND, Ritchie R, Bayes HK, Mitchell TJ and Evans TJ: IL-17 can be protective or deleterious in murine pneumococcal pneumonia. PLoS Pathog 14: e1007099, 2018.
16. Dallaire F, Ouellet N, Bergeron Y, Turmel V, Gauthier MC, Simard M and Bergeron MG: Microbiological and inflammatory factors associated with the development of pneumococcal pneumonia. J Infect Dis 184: 292-300, 2001.
17. Bazaz R: The effect of Streptococcus pneumoniae pneumonia on atherosclerosis (University of Sheffield, 2016).
18. Chen Y, Yu Q and Xu CB: A convenient method for quantifying collagen fibers in atherosclerotic lesions by ImageJ software. Int J Clin Exp Med 10: 14904-14910, 2017.
19. Livak KJ and Schmittgen TD: Analysis of relative gene expression data using real-time quantitative PCR and the 2(-Delta Delta C(T)) method. Methods 25: 402-408, 2001.
20. Sender V, Hentrich K, Pathak A, Ler ATQ, Embaie BT, Lundström SL, Gaetani M, Bergstrand J, Nakamoto R, Sham LT, *et al*: Capillary leakage provides nutrients and antioxidants for rapid pneumococcal proliferation in influenza-infected lower airways. Proc Natl Acad Sci USA 117: 31386-31397, 2020.
21. Corrales-Medina VF, deKemp RA, Chirinos JA, Zeng W, Wang J, Waterer G, Beanlands RSB and Dwivedi G: Persistent lung inflammation after clinical resolution of community-acquired pneumonia as measured by 18FDG-PET/CT imaging. Chest 160: 446-453, 2021.
22. Dommaschk A, Ding N, Tarres MT, Bittersohl LF, Maus R, Stolper J, Jonigk D, Braubach P, Lippmann T, Welte T and Maus UA: Nasopharyngeal colonization with Streptococcus pneumoniae triggers dendritic cell dependent antibody responses against invasive disease in mice. Eur J Immunol 47: 540-551, 2017.
23. Naura AS, Hans CP, Zerfaoui M, Errami Y, Ju J, Kim H, Matrougui K, Kim JG and Boulares AH: High-fat diet induces lung remodeling in ApoE-deficient mice: An association with an increase in circulatory and lung inflammatory factors. Lab Invest 89: 1243-1251, 2009.
24. Massaro D and Massaro GD: Apoetm1Unc mice have impaired alveologenesis, low lung function, and rapid loss of lung function. Am J Physiol Lung Cell Mol Physiol 294: L991-L997, 2008.
25. Torres A, Cilloniz C, Niederman MS, Menéndez R, Chalmers JD, Wunderink RG and van der Poll T: Pneumonia. Nat Rev Dis Primers 7: 1-28, 2021.
26. Brooks LRK and Mias GI: Streptococcus pneumoniae's virulence and host immunity: Aging, diagnostics, and prevention. Front Immunol 9: 1366, 2018.
27. Lagousi T, Basdeki P, De Jonge MI and Spoulou V: Understanding host immune responses to pneumococcal proteins in the upper respiratory tract to develop serotype-independent pneumococcal vaccines. Expert Rev Vaccines 19: 959-972, 2020.
28. Bartlett B, Ludewick HP, Misra A, Lee S and Dwivedi G: Macrophages and T cells in atherosclerosis: A translational perspective. Am J Physiol Heart Circ Physiol 317: H375-H386, 2019.
29. Siljan WW, Holter JC, Nymo SH, Husebye E, Ueland T, Aukrust P, Mollnes TE and Heggelund L: Cytokine responses, microbial aetiology and short-term outcome in community-acquired pneumonia. Eur J Clin Invest 48: e12865, 2018.
30. Dienz O and Rincon M: The effects of IL-6 on CD4 T cell responses. Clin Immunol 130: 27-33, 2009.
31. Bacci MR, Leme RCP, Zing NPC, Murad N, Adami F, Hinnig PF, Feder D, Chagas ACP and Fonseca FLA: IL-6 and TNF-α serum levels are associated with early death in community-acquired pneumonia patients. Brazi J Med Biol Res 48: 427-432, 2015.
32. Tanaka T, Narazaki M and Kishimoto T: IL-6 in inflammation, immunity, and disease. Cold Spring Harb Perspect Biol 6: a016295, 2014.
33. Yende S, D'Angelo G, Kellum JA, Weissfeld L, Fine J, Welch RD, Kong L, Carter M and Angus DC; GenIMS Investigators: Inflammatory markers at hospital discharge predict subsequent mortality after pneumonia and sepsis. Am J Respir Crit Care Med 177: 1242-1247, 2008.
34. Martens GW, Arikan MC, Lee J, Ren F, Vallerskog T and Kornfeld H: Hypercholesterolemia impairs immunity to tuberculosis. Infect Immun 76: 3464-3472, 2008.
35. Domon H and Terao Y: The role of neutrophils and neutrophil elastase in pneumococcal pneumonia. Front Cell Infect Microbiol 11: 615959, 2021.
36. Zernecke A and Weber C: Chemokines in atherosclerosis. Arterioscler Thromb Vasc Biol 34: 742-750, 2014.
37. de Jager Saskia CA, Bot I, Kraaijeveld AO, Korporaal SJA, Bot M, van Santbrink PJ, van Berkel TJC, Kuiper J and Biessen EAL: Leukocyte-specific CCL3 deficiency inhibits atherosclerotic lesion development by affecting neutrophil accumulation. Arterioscler Thromb Vas Biol 33: e75-e83, 2013.
38. Pfaff EM, Becker S, Günther A and Königshoff M: Dickkopf proteins influence lung epithelial cell proliferation in idiopathic pulmonary fibrosis. Eur Res J 37: 79-87, 2011.
39. Guo Y, Mishra A, Howland E, Zhao C, Shukla D, Weng T and Liu L: Platelet-derived Wnt antagonist Dickkopf-1 is implicated in ICAM-1/VCAM-1–mediated neutrophilic acute lung inflammation. Blood 126: 2220-2229, 2015.
40. Kim KI, Park KU, Chun EJ, Choi SI, Cho YS, Youn TJ, Cho GY, Chae IH, Song J, Choi DJ and Kim CH: A novel biomarker of coronary atherosclerosis: Serum DKK1 concentration correlates with coronary artery calcification and atherosclerotic plaques. J Korean Med Sci 26: 1178-1184, 2011.
41. Yao X, Gordon EM, Figueroa DM, Barochia AV and Levine SJ: Emerging roles of apolipoprotein E and apolipoprotein A-I in the pathogenesis and treatment of lung disease. Am J Respir Cell Mol Biol 55: 159-169, 2016.
42. Bazaz R, Francis S and Dockrell D: 407. The effect of streptococcus pneumoniae pneumonia on atherosclerosis. Open Forum Infect Dis 6: S207, 2019.
43. Naghavi M, Wyde P, Litovsky S, Madjid M, Akhtar A, Naguib S, Siadaty MS, Sanati S and Casscells W: Influenza infection exerts prominent inflammatory and thrombotic effects on the atherosclerotic plaques of apolipoprotein E-deficient mice. Circulation 107: 762-768, 2003.
44. Kaynar AM, Yende S, Zhu L, Frederick DR, Chambers R, Burton CL, Carter M, Stolz DB, Agostini B, Gregory AD, *et al*: Effects of intra-abdominal sepsis on atherosclerosis in mice. Crit Care 18: 469, 2014.
45. Brown AO, Mann B, Gao G, Hankins JS, Humann J, Giardina J, Faverio P, Restrepo MI, Halade GV, Mortensen EM, *et al*: Streptococcus pneumoniae Translocates into the Myocardium and forms unique microlesions that disrupt cardiac function. PLoS Pathog 10: e1004383, 2014.
46. Chen YC, Bui AV, Diesch J, Manasseh R, Hausding C, Rivera J, Haviv I, Agrotis A, Htun NM, Jowett J, *et al*: A novel mouse model of atherosclerotic plaque instability for drug testing and mechanistic/therapeutic discoveries using gene and microRNA expression profiling. Circ Res 113: 252-265, 2013.
47. Zivich PN, Grabenstein JD, Becker-Dreps SI and Weber DJ: Streptococcus pneumoniae outbreaks and implications for transmission and control: A systematic review. Pneumonia (Nathan) 10: 11, 2018.
48. Dion CF and Ashurst JV: Streptococcus pneumoniae. in *StatPearls* (StatPearls Publishing, 2021).

49. Ogino H, Fujii M, Ono M, Maezawa K, Hori S and Kizu J: In vivo and in vitro effects of fluoroquinolones on lipopolysaccharide-induced pro-inflammatory cytokine production. J Infect Chemother 15: 168-173, 2009.
50. Tilakaratne A and Soory M: Anti-inflammatory actions of adjunctive tetracyclines and other agents in periodontitis and associated comorbidities. Open Dent J 8: 109-124, 2014.
51. Steel HC, Theron AJ, Cockeran R, Anderson R and Feldman C: Pathogen- and host-directed anti-inflammatory activities of macrolide antibiotics. Mediators Inflamm 2012: 584262, 2012.
52. Sandgren A, Albiger B, Orihuela CJ, Tuomanen E, Normark S and Henriques-Normark B: Virulence in mice of pneumococcal clonal types with known invasive disease potential in humans. J Infect Dis 192: 791-800, 2005.
53. Bartlett B, Ludewick HP, Lee S, Verma S, Francis RJ and Dwivedi G: Imaging inflammation in patients and animals: Focus on PET imaging the vulnerable plaque. Cells 10: 2573, 2021.